PCCP

PAPER



Cite this: *Phys. Chem. Chem. Phys.*, 2017, **19**, 13664

# Binding site opening by loop C shift and chloride ion-pore interaction in the $GABA_A$ receptor model†

M. A. Michałowski, *[ab] S. Kraszewski[c] and J. W. Mozrzymas[a]

$GABA_A$ receptors ($GABA_A$Rs) are crucial in mediating inhibition in the adult mammalian brain. Although the kinetics of this receptor has been extensively studied, the molecular picture of interactions occurring at various channel conformations remains elusive. While electrophysiology combined with mutagenesis sheds light on the role of specific residues, ultrastructural studies reveal static structures which, in the case of $GABA_A$Rs, are limited to the $\beta_3$ homomer. To take advantage of the newest crystal structures of cys-loop receptors, a homology model of $\alpha_1\beta_2\gamma_2$ $GABA_A$R in the unbound closed state was built using a template of the homomeric glycine receptor in the closed state. The template model contained strychnine molecules at the binding sites which were removed and molecular dynamics was used to study the system relaxation. The modeled $GABA_A$R preserved the closed conformation. Two interfaces forming orthosteric binding sites ($\beta_2/\alpha_1$) exhibited opening due to the outward shift of loop C. Similar movement, although less pronounced, was observed at the $\alpha_1/\gamma_2$ (modulatory) interface. In contrast, interfaces $\alpha_1/\beta_2$ and $\gamma_2/\beta_2$ remained closed. The former one, due to interactions mediated mainly by loops C and F, affected the neighboring $\beta_2/\alpha_1$ interface leading to asymmetry between the orthosteric binding sites. Such interactions were not observed at the $\beta_2/\alpha_1$ interface preceded by a $\gamma_2$ subunit. As expected, in the channel pore, the conserved leucine gate and selectivity filter were present. However, an additional constriction was found at the top of the pore which differed from a typical hydrophobic channel gate as it consisted of charged residues. Interestingly, this site showed a capacity to trap chloride ions and to undergo conformation transition-like expansion, suggesting an impact on pore properties. In conclusion, our homology model faithfully reproduced major features of heteromeric $GABA_A$Rs offering insight into the underlying mechanisms of stabilizing the shut conformation and chloride ion interaction with the channel pore.

Received 1st February 2017,
Accepted 10th April 2017

DOI: 10.1039/c7cp00582b

rsc.li/pccp

## Introduction

$GABA_A$ receptors ($GABA_A$Rs) play a pivotal role in mediating inhibition in the adult mammalian brain and belong to the cys-loop family of pentameric ligand gated ion channels (pLGICs[1,2]). The most commonly occurring $GABA_A$R in the adult mammalian central nervous system (CNS) consists of two $\alpha_1$, two $\beta_2$ and one $\gamma_2$ subunit.[3,4] Each subunit comprises a particularly large extracellular domain, the transmembrane domain containing an ion pore with a channel gate and a selectivity filter and a relatively small intracellular domain.[5,6] The agonist binding sites are located in the extracellular domains at the interfaces between two neighbouring subunits (in $\alpha_1\beta_2\gamma_2$ receptors between $\beta_{2+}$ and $\alpha_{1-}$, Fig. S1, ESI†). The major physiological role of $GABA_A$Rs is to mediate rapid synaptic signalling. Indeed, the synaptic agonist transient is very short lasting (tenths of a millisecond), and elicits a highly dynamic response of post-synaptic $GABA_A$Rs.[7,8] Electrophysiological experiments, mostly at a macroscopic but also at the single channel level, provided a wealth of information on the kinetics of these receptors[17–20] which shows that, although some similarities to the cys-loop counterparts (5-HT3, AChR or GlyR) are well established, $GABA_A$R functioning shows also profound differences, both at the qualitative and quantitative level, including *e.g.* rapid desensitization, specific mechanism of deactivation or various single-channel conductances. These differences are not surprising since subunits belonging to different types of cys-loop receptors show a relatively

[a] *Laboratory of Neuroscience, Department of Biophysics, Wrocław Medical University, ul. Chałubińskiego 3a, 50-358 Wrocław, Poland*
[b] *Department of Physiology and Molecular Neurobiology, University of Wrocław, ul. Sienkiewicza 21, 50-335 Wrocław, Poland. E-mail: michalmichalowski@uwr.edu.pl*
[c] *Department of Biomedical Engineering, Faculty of Fundamental Problems of Technology, Wroclaw University of Science and Technology, Wyb. Wyspiańskiego 27, 50-370 Wrocław, Poland*

† Electronic supplementary information (ESI) available. See DOI: 10.1039/c7cp00582b

low homology of their sequences (ESI,† Fig. S1). Moreover, $GABA_A$Rs built with different types of subunits (especially among α types or receptors containing γ or δ subunits) may show dramatic kinetic and pharmacological differences.[21–23] These observations clearly demonstrate that in spite of a common structural phenotype of cys-loop receptors (and $GABA_A$R subtypes in particular), relatively minor structural differences within specific subunits may result in marked alterations in receptor functioning. An extensive body of evidence about the role of specific amino acid residues in $GABA_A$R function was obtained by combining patch- and voltage-clamp recordings and mutagenesis.[24–28] However, a prerequisite to explore the structure–function relationship is to precisely determine the receptor's structure and to infer the molecular mechanisms underlying the conformational transitions. Two methods are extensively used in high-resolution studies of the cys-loop receptor structures: X-ray crystallography and cryo-electron microscopy. The first technique proved to be particularly successful in determining the structure related to a cys-loop family member, the acetylcholine binding protein (AChBP, corresponding to the extracellular domain, rendering it easier to crystallize) with an unprecedented resolution of 2.7 Å.[29] Determination of the complete AChR structure, although at a lower resolution, was achieved first by Miyazawa *et al.* (resolution 4.0 Å)[30] and then by Unwin (resolution 4.0 Å).[16] An important step forward was to obtain crystal structures of receptors in presumed closed and open states for ELIC[31] and GLIC,[32] respectively, providing thus a structural snapshot of open and closed states of these receptors. However, these bacterial receptors show structural differences and a low homology with mammalian cys-loop receptors. Recently, Althoff *et al.*[11] have determined the structure of the *C. elegans* glutamate receptor permeable to chloride ions (GluCl) in two distinct conformations offering a new insight into its structure–function relationship. In the past couple of years or so, a number of seminal papers on the cys-loop receptor structure have been published. Besides the paper by Althoff *et al.* on a GluCl receptor, the structure of a glycine receptor was thoroughly investigated.[9,10] In particular, Du *et al.* have determined the structure of the zebrafish $\alpha_1$ homomeric glycine receptor (GlyR in three distinct conformations: open, closed (with strychnine) and presumed desensitized state). Hassaine *et al.*[13] have determined the X-ray structure of the mouse 5-HT3 receptor in the closed state. In 2014, Miller & Aricescu[15] published the first crystal structure of $GABA_A$R for the $\beta_3$ subunit homopentamer. However, the structure for physiologically occurring heteropentamers is lacking. Although structural description of the $GABA_A$R homopentamer is an important breakthrough, heteropentamers operate differently in several respects such as the number of binding sites, lateral intersubunit interactions, manifested by *e.g.* a strong regulatory role of the γ subunit (resulting in profound differences between αβ and αβγ receptors) and by modulation of GABA binding sites by benzodiazepines which bind to a site distant from orthosteric binding sites at $GABA_A$R macromolecules (between $\alpha_+$ and $\gamma_-$ subunits). It is thus a major challenge to infer the structure of $GABA_A$R heteropentamers, *e.g.* of its most common subtype $\alpha_1\beta_2\gamma_2$. While crystallization of these receptors still poses major difficulties, homology modelling appears to be an optimal tool, especially when the structure of relatively highly homologous receptors has been described. Clearly, the β3 homopentamer as the structure template appears to be the best starting point for this approach. This structure was already used to investigate the mechanisms of allosteric modulation[33,34] but the main disadvantage is that the structure is available only for one conformation whose functional interpretation is not clear. Although GluCl is less structurally similar to $GABA_A$Rs, its structure is available for different conformations. Recently, the GluCl structure was used as a modelling template[35] to elucidate modulatory actions of anaesthetics and ethanol[36] and to investigate insect GABA receptors.[37] The "classic" structures such as – AChBP and nAChR are still used as templates in studies on $GABA_A$Rs. For instance, Sander *et al.*[38] investigated a model of the extracellular domain of $GABA_A$R and Carpenter and Lightstone[39] modelled the agonist binding path. In the present study we propose a new homology model of the $\alpha_1\beta_2\gamma_2$ $GABA_A$R based on the structural template of GlyR[10] and examine structure relaxation using molecular dynamics simulations taking into account the water/lipid surrounding. This choice was based on a relatively high homology between $GABA_A$R and GlyR subunits (Fig. 1) and the fact that the structure of GlyR was resolved in different conformations, including open and inactive states. Especially the latter argument was considered to be important as it makes these modelistic investigations potentially more versatile, offering in the future a perspective for in depth molecular dynamics investigations into the molecular mechanisms of conformational transitions. In the present study, we report that such a $\alpha_1\beta_2\gamma_2$ $GABA_A$R model in the closed conformation is characterized by a high stability reproducing major structural features of these receptors. Interestingly, molecular dynamics simulations based on this model revealed striking differences between orthosteric GABA ($\beta_{2+}/\alpha_{1-}$), benzodiazepine ($\alpha_{1+}/\gamma_{2-}$), and other interface sites ($\alpha_{1+}/\beta_{2-}$ and $\gamma_2/\beta_{2-}$) considered in the model. Namely, following removal of constraints, the GABA binding site tended to open (uncapping), the benzodiazepine site remained partially open whereas the latter ones showed relaxation towards a closed conformation indicating that lateral intersubunit interactions play a key role in the functioning of this receptor. In addition, we have detected an extra gate-like structure in the TMD which underwent widening as a consequence of interaction with chloride ions. In conclusion, our new homology model of $GABA_A$R is characterized by a high stability and reproduces well its structural features offering potential for in-depth modelistic investigations of conformational transitions (Table 1).

# Methods

### Template selection

Several cys-loop pLGIC structures in closed,[11,13,31] only one in open[10] and three in partially open/desensitized[10,12,15] states are available (Table 1). To ensure the best template selection for the model building process custom-made analysis of these structures was performed. The glycine receptor (GlyR) in the

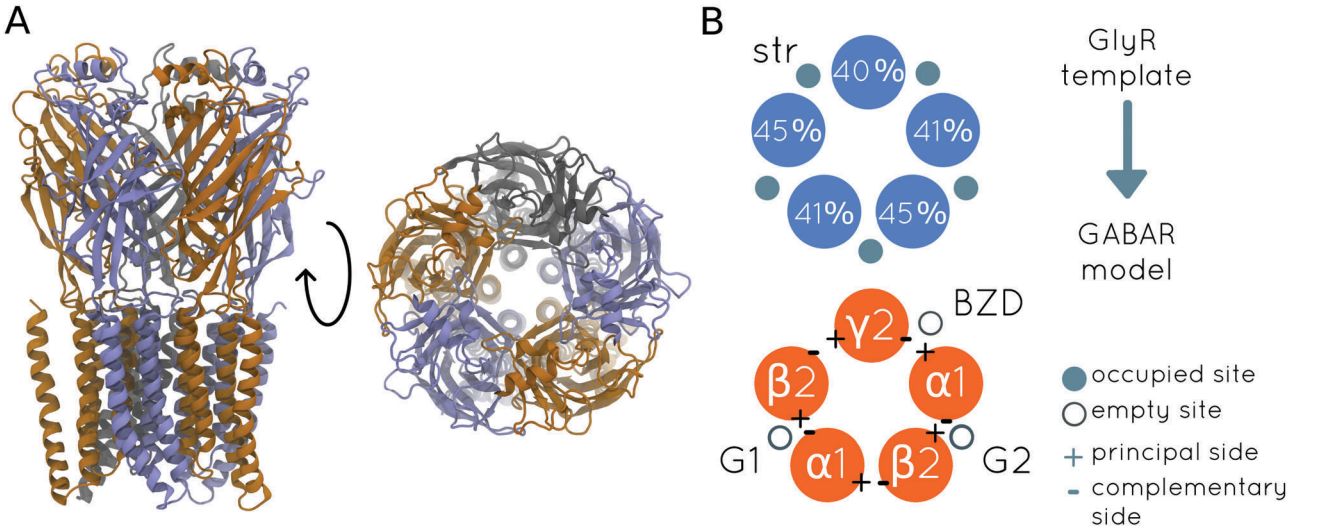


Fig. 1 General topology of GlyR and $GABA_AR$. (A) Cartoon representation of $GABA_A$ receptor, view from the side (perpendicular to the lipid membrane) and top. $\alpha_1$ subunits in blue, $\beta_2$ subunits in orange, $\gamma_2$ subunit in grey. (B) The cryo-electron microscopy structure of GlyR (Du *et al.* 2015) was used to build the $\alpha_1\beta_2\gamma_2$ $GABA_AR$ homology model. Values at GlyR homomeric subunits indicate sequence identity with respective $GABA_AR$ subunits. In the GlyR template all binding sites are occupied by strychnine (str) molecules, whereas in the $GABA_AR$ model both (first – G1, and second – G2) GABA and benzodiazepine (BZD) binding sites are empty. Each intersubunit interface has its principal (+) and complementary side (–). One of the key features of the principal side is that it covers the intersubunit interface by its loop C.

Table 1 Available crystal structures of cys-loop receptor family members. State categorization according to ref. 10

| Closed | Open | Partially open/desensitized |
|---|---|---|
| str-GlyR[9,10] | gly-GlyR[10] | gly/ivm-GlyR[10] |
| apo-GluCl[11] | | glu/ivm-GluCl[12] |
| 5-HT3R[13,14] | | β3-GABAR[15] |
| nAChR[16] | | |

strychnine bound closed conformation (ESI,† Fig. S2A) was selected as a template for the following reasons: (i) GlyR is the only cys-loop receptor captured in three main conformations,[10] and (ii) its structure is of high quality and sequence identity to the respective $GABA_AR$ subunits is relatively high: $\alpha_1$ 41% ($GABA_A$ $\beta_3$ 41%, GluCl 35%), $\beta_2$ 45% ($GABA_A$ β3 90%, GluCl 40%), $\gamma_2$ 40% ($GABA_A$ β3 44%, GluCl 33%). For comparison with other subunits from other cys-loop family members see the ESI,† Fig. S1. The GlyR closed state (blocked by competitive antagonist strychnine) was selected and it is expected that after antagonist removal, structural movements related to macromolecule relaxation will concern mainly the binding site area and subunit interfaces. Selection of the GlyR template also allows the preparation of a $GABA_AR$ model for future studies, in open and desensitized states, ensuring reliability of comparative analysis.

### Sequence alignment

An extended set of cys-loop family pLGICs was selected for sequence alignment: all human $GABA_AR$ subunit sequences: α (1 : 6), β (1 : 3), δ, ε, γ (1 : 3), π, ρ (1 : 3), θ, all human GlyR subunit sequences: α (1 : 4), β, *C. elegans* GluCl α and β subunit sequences, all taken from the UniProt database[40] and selected sequences of available pLGIC crystal structure constructs: GlyR,[10] GluCl[11] and $\beta_3$ $GABA_AR$[15] extracted from the RCSB PDB database.[41] Initial alignment was done using Clustal Omega software[42] and manually refined according to experimental data and structural information. Two main areas of manual refinement were the loop F and the intracellular domain. Because of the absence of an intracellular domain in the crystal structure of GlyR, an AGT tripeptide was placed in between the M3 and M4 α-helices of the transmembrane domain. In loop F, the residues were aligned according to the conserved W*R(E, D) motif in the initial part and V*V in the ending part of the loop. Both manual changes were additionally based on comparative analysis of crystal structures to ensure correct α-helix starting/ending residue alignment positions. Fig. S3 (ESI†) shows the alignment of selected sequences. The secondary structure of the $\alpha_1$ $GABA_AR$ subunit (ESI,† Fig. S3) was predicted with JPred software.[43]

### Model building and quality evaluation

A closed state $GABA_AR$ model was built using Modeller 9.15.[44] A single template of GlyR in the strychnine bound conformation[10] was used. Special patches were used to ensure correct disulphide bonds. 256 models were constructed using the highest precision settings. No additional loop refinement was performed since further relaxation was done using molecular dynamics simulations.

The quality of multiple models was estimated using both visual inspection and quality measures like molpdf,[44] qmean score[45] and Rampage assessment.[46] The top 25% previously generated models jointly scored by molpdf and dope were selected for the estimation of quality. Qmean server is a complex method for model quality assessment but is not yet optimized for macromolecules containing large transmembrane domains.[45] The scores of such structures may be underestimated because

 

of incorrect assessment of hydrophobic interactions resulting from not taking into consideration the presence of lipid membranes.[45] All models achieved similar results, slightly above 0.5 qmean score, which means that this method is not sufficient to indicate the best model among similar ones. Structures were also assessed with Rampage to exclude models with a high amount of residues in unlikely conformations. The final model (ESI,† Fig. S2B) was selected according to all scoring functions. The selected model had both good DOPE and molpdf scores indicating relatively small divergence from the template and an energetically favourable conformation. Qmean and Rampage evaluation showed no major deviations from the expected quality.

### Molecular dynamics

An all-atom molecular dynamics (MD) system was prepared using CHARMM GUI[47] as well as input configuration files and protein topology[47,48] for NAMD 2.11[49] which was used to perform further simulations. A previously built $\alpha_1\beta_2\gamma_2$ $GABA_AR$ model was placed into a 670 POPC bilayer and solvated with a 25 Å slab of TIP3 water molecules.[50,51] NaCl ions were added to achieve physiological 0.15 M concentration. All default values of parameters were used except for prolongation of the final equilibration step (CHARMM GUI step 6.6 – up to stable protein RMSD) and lowering the Langevin temperature damping coefficient to 0.1 ps by changing the Langevin piston period to 200 fs in the production run. The complete energy minimization and equilibration protocol consisted of six steps of constrained MD simulations. These constraints have been lowered in each subsequent simulation gradually releasing the system. In addition, the first step was preceded by energy minimization using a standard NAMD procedure (based on conjugate gradient and line search algorithms). The total length of the simulation exceeded 150 ns.

### Ion docking and molecular dynamics

To obtain a new system with ion docked in TMD, final coordinates from MD simulations were taken and a chloride ion was positioned using Autodock Vina software.[52] The best docking pose, according to Vina quality assessment methods, was selected. Besides putting a chloride ion in the site and moving one water molecule from the ion pore back to the solution, no changes in the system were made. A complete system was minimized and equilibrated in a two-step manner: first, both the protein and chloride ion atom positions were constrained (for about 2 ns), in the second step, the protein constraints were removed (for about 3 ns). This three-step preparation allowed the removal of any natural tensions caused by docking and was followed by a 20 ns long production run.

### Visualization and analysis

All visualizations were made using VMD 1.9 software.[53] Analyses of the results were done using VMD tcl scripts[53] and custom Python 3.5 scripts using Nump,[54] Pandas,[55] Matplotlib[56] and Seaborn[57] packages. The ion pore dimensions were estimated using the Hole program.[58]

## Results

### $GABA_AR$ $\alpha_1\beta_2\gamma_2$ structural homology model

In order to elucidate the structural features of $GABA_AR$ $\alpha_1\beta_2\gamma_2$ in the closed conformation, a homology model was created using the structure of closed GlyR with bound strychnine (competitive antagonist present in all five intersubunit binding sites) as a template.[10] Then the strychnine molecules were removed and the system was allowed to relax in our molecular dynamics simulations and, finally, a stable closed $GABA_AR$ conformation was revealed.

The $GABA_A$ receptor of interest consists of five subunits (two $\alpha_1$, two $\beta_2$ and one $\gamma_2$, see Fig. 1 for the general topology of $GABA_AR$ and GlyR) and, as mentioned in the Introduction, each subunit contains an extracellular domain (ECD) and a transmembrane domain (TMD) as well as the intracellular domain which in the present modelling is neglected (it was not present in the template structure). The topology of the $\alpha_1\beta_2\gamma_2$ $GABA_A$ receptor based on homology modelling is presented in Fig. 2, where major α-helices, β-strands and loops are highlighted. Each extracellular domain contains a set of β-strands numbered (from 1 to 10) according to their appearance order starting from the N-terminus in the extracellular compartment. Strands β1, β2, β3 and β6 of the complementary subunit belong to the inner sheet at the intersubunit interface. Strands β5 and β8 can also be classified as belonging to the inner sheet and the former one is delimiting the sheet from the side of the inner cavity whereas the latter one – from the ECD side exposed to solvent (Fig. 2). Strands β4, β7, β9 and β10 of the principal subunit belong to the outer β-sheet. Interestingly, a high conservation level was observed in all transmembrane α-helices (M1, M2, M3, M4), but not on the loops connecting them (ESI,† Fig. S3). This suggests a common frame of the ion pore and a receptor-specific mechanism of signal transduction from the ECD to the TMD as these loops (especially pre-M1 and M2–M3) are known to play a key role in this process. In addition, in the ECD, β-stands from the 4th to the initial segment of the 8th one showed a higher conservation level than β-strands 1, 2, 8, 9 and 10 (ESI,† Fig. S3). The first group is located in the inner part of the domain, while the latter one is more solvent exposed and interacts more frequently with the ligand (Fig. 2A). Thus, it can be speculated that the second group, due to higher variability, could be involved in ligand specific interactions while more conservative β-strands might be involved in a signal transduction mechanism from the ECD to the TMD that is highly conserved in all receptor types. Key areas surrounding the aromatic box are referred to as loops (A–F) although this nomenclature is somehow misleading as ''loops'' D and E are pieces of the β strands β2 and β6, respectively, whereas the remaining loops are unstructured connectors between respective strands (A: β4–β5, B: β7–β8, C: β9–β10, F: β8–β9, Fig. 2A). It is expected that a high content of α-helices and β-strands with few unstructured loops and low solvent exposure will constrain the structure mobility whereas large unstructured loops (*e.g.* loop C or F) exposed to solvent will show a considerably larger propensity for movements. Importantly, the mobility of these loops appears to be an important

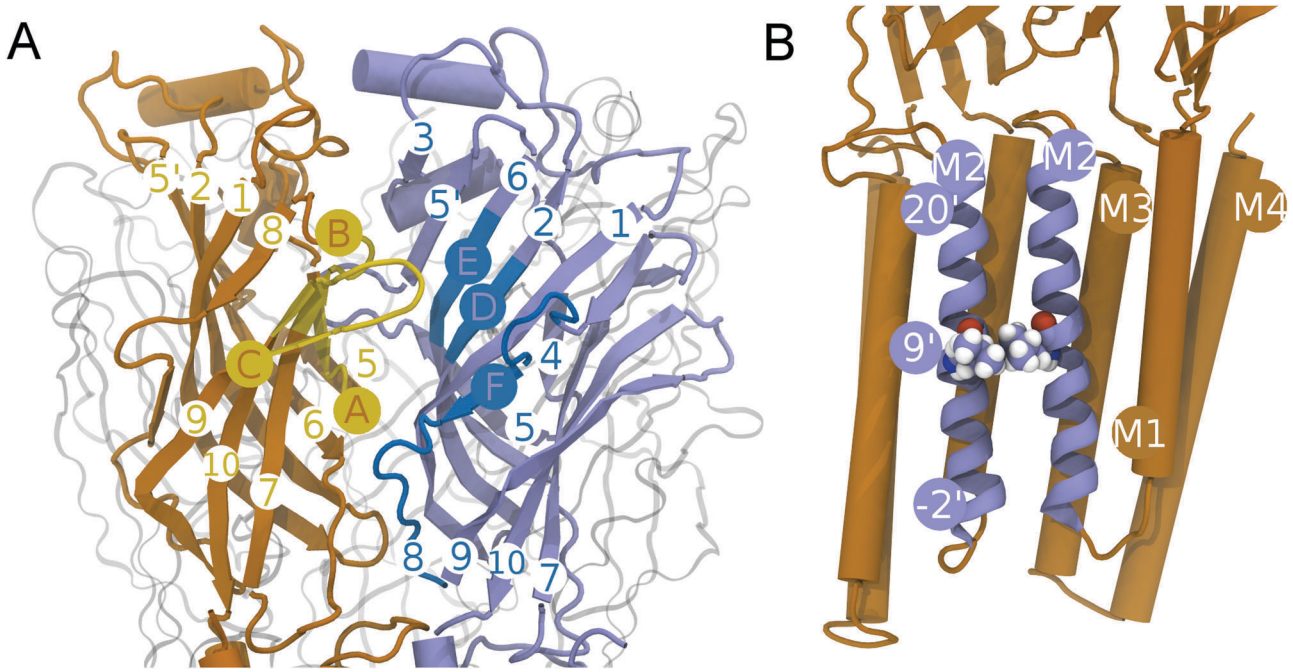


Fig. 2 Key loops, β-strands and α-helices of the $\alpha_1\beta_2\gamma_2$ $GABA_AR$ model. (A) Extracellular domain (ECD) of $\alpha_1\beta_2\gamma_2$ $GABA_AR$. Principal (orange) and complementary (blue) subunits shown in cartoon representation. Remaining subunits shown in the background for clarity. Key loops marked A–C (shown only in the principal subunit) and D–F (shown only in the complementary subunits). The complete range (1–10) of β-strands is presented on both subunits. High solvent exposure of loop C and loop F and β-strand 8. Loop F and β8 are showing a high proportion of unstructured loops with respect to β-strand suggesting high mobility of this region. (B) Transmembrane domain (TMD) of $\alpha_1\beta_2\gamma_2$ $GABA_AR$. View from inside of the ion pore, only two subunits are shown. M2s are lining the pore (blue) with the channel gate made of five leucine residues at the 9′ residue level shown in van der Waals representation. The remaining part of the TMD is made of M1s, M3s and M4s. In the model, M3s and M4s are connected with a short peptide which substituted the intracellular domain.

factor in setting the macromolecule capacity to bind the agonist – an issue that will be considered in detail in MD studies of this work (see Sections 3.3 and 3.4). TMD is formed by α-helices (four in each subunit) named M1, M2, M3 and M4 (Fig. 2B) connected with loops (M1–M2 and M2–M3) or by an intracellular domain (M3–M4, not present in the model). The ion pore is made of five M2 α-helices (one from each subunit) and their residues are often numbered from −2′ at the bottom up to 20′ at the top of the pore (Fig. 2B). The channel gate is located in the middle of the TMD and is made of five leucine residues (showed in van der Waals representation in Fig. 2B). Besides this channel gate two additional narrow rings with radii larger than in the case of the leucine gate were found in our model: the first at the bottom (−2′, 2′ area) which corresponds to the selectivity filter and the second one at the pore top (20′). Whereas the selectivity filter is a well-known channel structural domain, the role of the second pore narrowing was not clear and was therefore subjected to detailed examination using molecular dynamics simulations (see Section 3.5).

### Tertiary and quaternary structure dynamics

In the template structure (GlyR), all intersubunit interfaces in the extracellular domain are forming functional binding sites and originally were occupied by strychnine (ESI,† Fig. S2A). However, in the heteropentameric $\alpha_1\beta_2\gamma_2$ $GABA_AR$ this symmetry is broken and therefore respective intersubunit interfaces are expected to show differences both at the structural and functional level (ESI,† Fig. S2B). In the classic heteropentameric $GABA_AR$ (Fig. 1), two orthosteric binding sites are present at the interfaces between neighbouring $\beta_2$ principal and $\alpha_1$ complementary subunits ($\beta_{2+}/\alpha_{1-}$ interface) and one allosteric (BDZ) binding site is present at the interface between $\alpha_{1+}$ principal and $\gamma_{2-}$ complementary subunits.[22]

MD simulations of $GABA_AR$ in the ligand free closed state lasted for more than 150 ns allowing substantial relaxation movements induced by removal of the competitive antagonist (strychnine) from the binding sites to be observed. Within the first 25 ns a rapid increase in the root mean square displacement (RMSD) function was observed (Fig. 3) which is typical for the equilibration phase. Next, a drift of RMSD value was seen for approximately 75 ns (Fig. 3) which reflected mainly the intersubunit adaptation rearrangements and interactions of the upper part of ECD with solvent. After approximately 100 ns, the RMSD value reached a steady value (Fig. 3) indicating that most of the intense movements related to relaxation were accomplished. However, at this stage, we have observed in our MD simulations an oscillatory-like movement of loop C in the $\alpha_1$ subunit neighbouring $\gamma_2$ subunit, indicating an unstable state of this element (see below in Section 3.3 on C loop movements). As expected, following strychnine removal, the pore retained its closed conformation (see also below considerations of the pore geometry, Section 3.5). To describe the most displaced areas

 

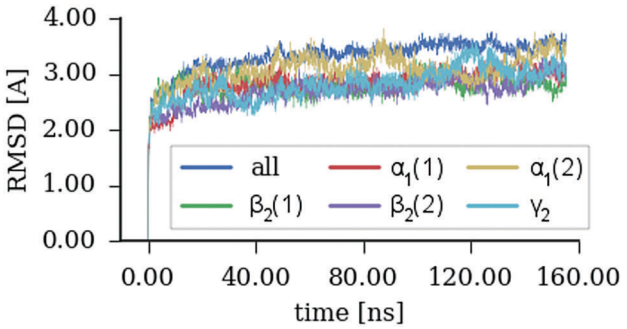


Fig. 3 Relaxation of the $\alpha_1\beta_2\gamma_2$ $GABA_AR$ homology model. Time course of RMSD (root-mean-square deviation of atomic positions) after releasing the constraints ($t$ = 0, at the same moment strychnine molecules were removed) for respective subunits and the whole receptor during molecular dynamics simulations. Note that within 20 ns rapid equilibration, characterized by a fast onset of RMSD, took place which was followed by approximately 80 ns of a slow increase before the system reached the stability phase.

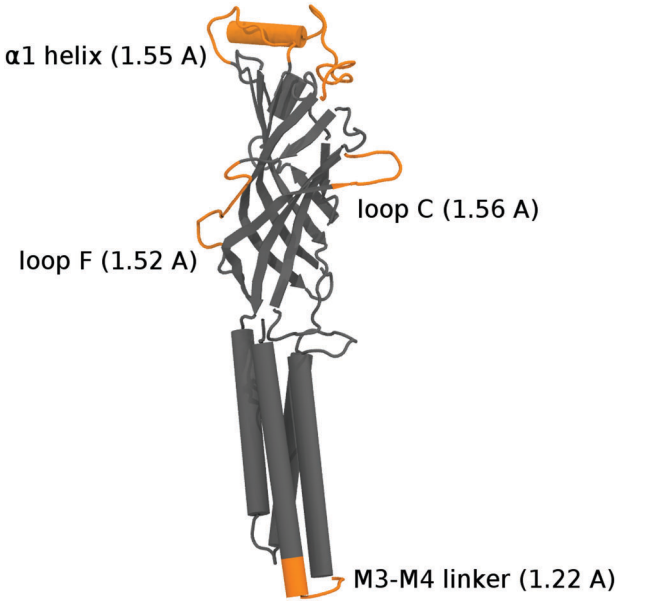


Fig. 4 Most mobile fragments of the $\alpha_1\beta_2\gamma_2$ $GABA_AR$ homology model. RMSF (root-mean-square fluctuation of atomic positions, *i.e.* value describing a movement of atoms relative to their mean positions). In the figure, mean values of RMSF (during MD simulations) are reported for the most mobile regions which are shown in orange. The most extensive movement was observed in solvent exposed regions and areas involved in ligand binding and/or forming intersubunit interfaces.

relative to the template and the most mobile macromolecule regions, RMSD and root mean square fluctuation (RMSF) per residue were computed (ESI,† Fig. S4A and B). The highest values of these parameters were found at the top part of the ECD, at the bottom part of the TMD and on loops C and F (Fig. 4). The high mobility of the protein N termini regions was mainly due to interactions with the solvent and the relatively high flexibility of these regions mainly due to non-structured loops. Loops C and F are involved in ligand binding,[59] thus it seems interesting to describe in detail their relaxation movements.

### Loops C and F in orthosteric and allosteric binding sites

As already mentioned, unstructured and exposed to solvent, loops C and F are good candidates to undergo substantial movements (Fig. 2A). Indeed, loop C has been implicated in agonist capping,[60,61] the process resulting in affinity increase associated with conformational changes of the macromolecule. At the starting point of our simulations, all the loops C were in the closed (capped) conformation. This could be expected as strychnine is a competitive antagonist which largely mimics the properties of orthosteric ligands which are widely believed to be capped by loop C. It is worth pointing out that the two orthosteric binding sites are not equivalent in the present model as the principal subunits ($\beta_2$) are flanked by different subunits (in Fig. 1, in the first binding site, the $\beta_2$ subunit is flanked by the $\gamma_2$ subunit whereas in the second binding site – by the $\alpha_1$ subunit). Our MD simulations predicted that at both orthosteric binding sites (between $\beta_{2-}$ and $\alpha_{1+}$ subunits) the C loops moved away from their initial positions giving rise to opening of the binding site (Fig. 5A and B). Movements of loops C took place in our simulations within energy minimization steps, constrained equilibration simulations and during the first 15–20 ns after removal of constraints. Although at the two binding sites movements of the C loops were similar, there were also some differences. Whereas at the first binding site, the moving C loop largely maintained its shape, at the second one, a widening of the upper part of this loop took place (Fig. 5A–C). Our analysis revealed a negligible interaction with the $\gamma_2$ subunit in the case of the first binding site while in the case of the second one, we detected an interaction between the flanking $\alpha_1$ (at its "+" side) and the principal $\beta_2$ subunit (at its "−" side) and a resulting movement (see also discussion of the underlying mechanism in Section 3.4). Namely, the flanking $\alpha_1$ subunit dragged neighbouring $\beta_2$'s loop C *via* loop F (Fig. 5E) and β-strand β9 which also showed some movement (Fig. 5E). Thus, upon relaxation following strychnine removal, loop C movement may be divided into two phases: (i) vertical shift away from the binding site cavity (removal of the steric block – capping) that would allow the ligand to enter the binding site, and (ii) loop widening by loosening the strand, which broadens the binding site, but also, due to increased solvent interaction, loop C becomes more flexible, allowing more efficient ligand fitting (this occurs at the second orthosteric binding site interface preceded by the $\alpha_1$ subunit).

Besides the orthosteric binding sites there are additionally two interfaces containing the $\alpha_1$ subunit which might potentially bind the ligand in our model: $\alpha_{1+}/\beta_{2-}$ and $\alpha_{1+}/\gamma_{2-}$ (Fig. 1). It is generally believed that in $GABA_ARs$ the $\alpha_{1+}/\beta_{2-}$ interface does not form any ligand binding site whereas the latter one is commonly implicated as an allosteric binding site (for BDZs). It is interesting to confront these premises with predictions of our model. Our MD simulations revealed that at the $\alpha_{1+}/\beta_{2-}$ interface an extensive movement of loop C is taking place leading to the closure (capping) of the binding site (Fig. 5D). This movement of loop C is accompanied by a complementary loop F shift in the $\beta_2$ subunit at the second orthosteric binding site which

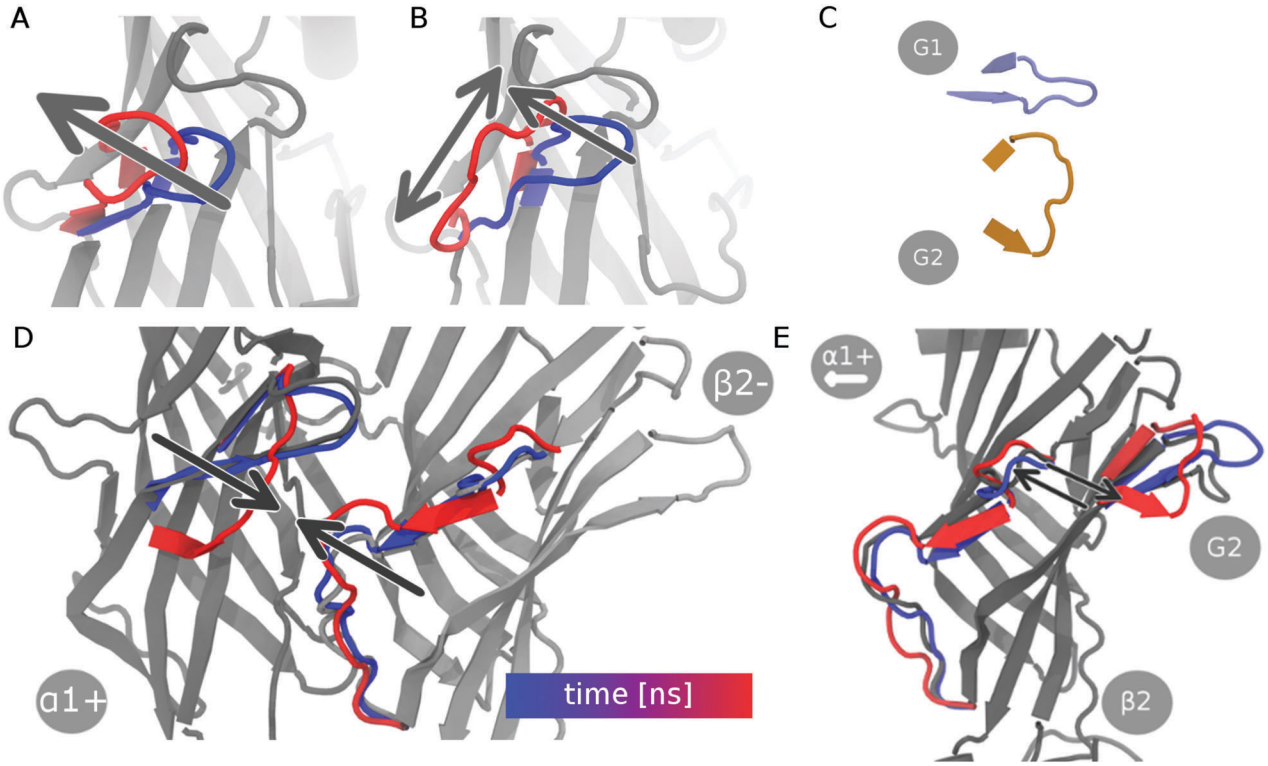


Fig. 5 Tertiary structural movements at intersubunit interfaces. Starting homology model structure is presented in grey. Elapsed time is color coded: starting phase in blue, late phase in red. Arrows indicate principal directions of loop movements. (A) At the first GABA binding site (Fig. 1) loop C of the $\beta_2$ subunit opens showing the interior of the orthosteric binding site. Effect of interaction with the preceding $\gamma_2$ subunit is negligible. (B) At the second GABA binding site, the loop C of the $\beta_2$ subunit shows a similar upward shift as in the first site but also widens. At this site interaction with predating $\alpha_1$ subunit is strong (see the Results section). (C) Difference of loop C shape between the first and the second binding sites shown in (A and B). (D) Mechanism of closing the $\alpha_{1+}/\beta_{2-}$ nonbinding interface: $\alpha_1$ subunit loop C extends toward $\beta_2$ subunit loop F. (E) Loop F in the $\beta_2$ subunit of the second GABA binding site (shown in D) drags loop C which results in widening its upper part and modulation of the 2nd binding site shape (shown in B).

further ''seals'' the interface disallowing ligand binding. Thus, our model nicely predicts that whereas the orthosteric binding sites ($\beta_{2+}/\alpha_{1-}$) relax towards a conformation permissive for ligand access, the $\alpha_{1+}/\beta_{2-}$ one assume conformation preventing the access of agonists. At the ($\alpha_{1+}/\gamma_{2-}$) interface, initially loop C opened, similar to what was observed at the orthosteric binding sites but then it moved close to the initial position with its upper part widened and, as mentioned above, showed some fluctuations. This behaviour of loop C suggests that, in the resting state, the allosteric binding site may oscillate between open and closed states which is defined as a partially open conformation. The loop C of the $\gamma_2$ subunit remained in closed position, as expected, and did not show any extensive interaction with the preceding $\alpha_1$ subunit.

### Loops C, F and D interactions in non-binding inter subunit interfaces

As discussed above, our model simulations predict that the $\alpha_{1+}/\beta_{2-}$ interface remains inaccessible for ligands in contrast to orthosteric binding sites. It seems interesting to have a closer look at local interactions leading to the $\alpha_{1+}/\beta_{2-}$ interface closure. Movement of loop C at the $\alpha_1$ subunit is attenuated by interaction between three charged aminoacids: Arg163 located on the β7–β8 loop of the $\alpha_1$ subunit, Arg117 at the β5 strand of the $\beta_2$ subunit and Glu208 on the loop C of the $\alpha_1$ subunit (Fig. 6A). Both arginines are forcing loop C to close the interface, the one from the $\alpha_1$ subunit extends the loop by distorting the β9 strand and the one from the $\beta_2$ subunit drags it toward the complementary subunit. However, these interactions are not stable because the two arginine residues are too far from the glutamate functional group to create a strong salt-bridge interaction and for this reason some movement of these residues was observed. At the initial phase of our simulations, the Arg163$\alpha_1$ functional group was closer to the Glu208$\alpha_1$ functional group for 74% of the simulation time, however, at the later phase when the structure tended to stabilize, Arg163α1 was closer to Arg117$\beta_2$. In addition, we observed that the structures containing the two arginines may show temporary interactions with Glu208 but this situation is only possible when the interaction involves the backbone carbonyl group of Arg163 rather than its functional group. Thus the two arginines and Glu208 tend to form a local network of electrostatic interactions which, on one hand, is stabilizing loop C at a position closing the cavity but on the other hand, the network is not fully stable as its structure precludes the formation of strong salt bridges.

From the side of the $\beta_2$ subunit, the main mobile element able to affect the putative binding site at this interface ($\alpha_{1+}/\beta_{2-}$, Fig. 1) is loop F. Importantly, this loop is connected to the rigid

 

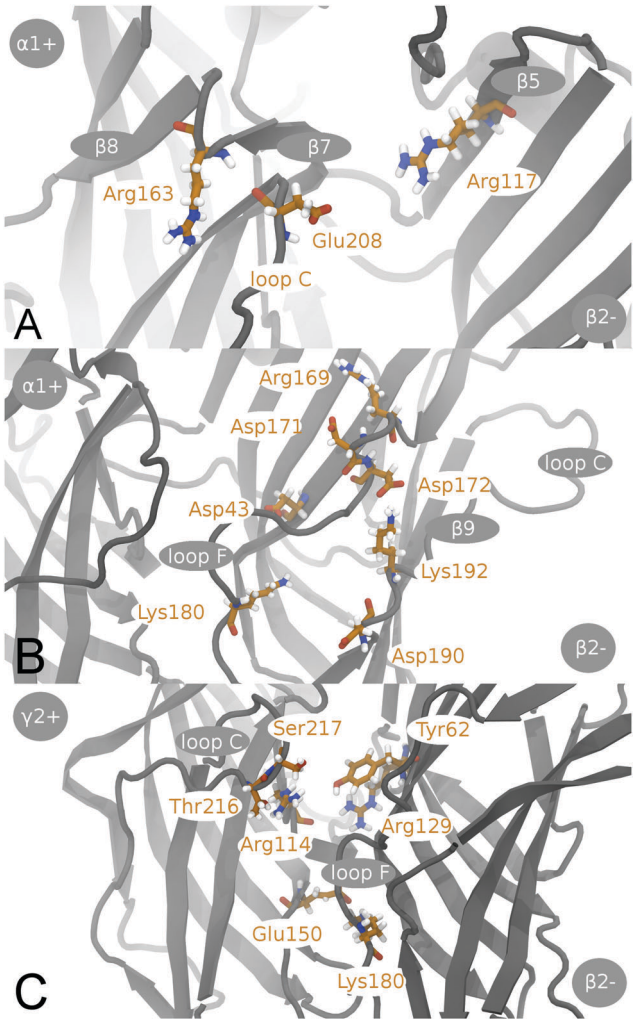


Fig. 6 Residue-level interactions at non-binding interfaces. (A) Snapshot of Arg163$\alpha_1$ in contact with Glu208$\alpha_1$ and Arg117$\beta_2$ at the $\alpha_{1+}/\beta_{2-}$ interface. Arg163$\alpha_1$ interacts with the glutamate Cβ carbonyl group allowing loop C to be dragged by Arg117$\beta_2$ from the complementary side closing the interface. (B) Arg169$\beta_2$ and Asp171$\beta_2$ interaction positions Asp172$\beta_2$ toward Lys192$\beta_2$. This residue is connected with loop C of the neighbouring binding site. Lys180$\beta_2$ breaks interaction with Asp190$\beta_2$ and shifts toward Asp43$\beta_2$ which causes the whole loop F to move and close this intersubunit interface. (C) Snapshot of key residues in the $\gamma_{2+}/\beta_{2-}$ interface. Both Ser217$\gamma_2$ and Thr216$\gamma_2$ from loop C are interacting with loop A Arg114$\gamma_2$ functional group. Arg114$\gamma_2$–loop E Arg129$\beta_2$ interaction is presented at the bottom of the interface.

strand β9 which, in turn, leads to loop C which is supposed to directly interact with the ligand at the second orthosteric binding site. Within the $\beta_2$ subunit a strong interaction in the middle of loop F is formed by Arg169$\beta_2$ and Asp171$\beta_2$ which position Asp172$\beta_2$ to face Lys192$\beta_2$ located on the β9 strand (Fig. 6B). Similar contact is observed between Lys180$\beta_2$ (loop F) and Asp190$\beta_2$ (β9 strand) but within the time of our simulations this interaction is switched to Asp43$\beta_2$ (loop G) which is associated with repositioning of loop F toward loop C resulting in closure of the interface (Fig. 6B). Thus, closure of the cavity at the $\alpha_{1+}/\beta_{2-}$ interface is a consequence of a concomitant C loop stabilization and F loop shift due to local electrostatic interactions. It is important that the above mentioned interactions between Arg163$\alpha_1$, Glu208$\alpha_1$ and Arg117$\beta_2$ represent an intersubunit interaction which is conveyed to the principal subunit $\beta_2$ *via* strand β5 (on which Arg117 is located, Fig. 6A) and neighbouring it strands β1, β2 and β6. From the solvent exposed side of the receptor this is transferred by interaction between Asp172$\beta_2$ and Lys192$\beta_2$ that leads to β9 strand shift due to interaction with loop F. Indeed, this interaction between $\alpha_1$ and $\beta_2$ subunits results in some movement of this sheet in the principal subunit $\beta_2$ providing a likely explanation for a widening of loop C at the second binding site (Fig. 5B), the phenomenon that was basically absent at the first binding site.

The second intersubunit interface, which is known not to form any binding site, is located between $\gamma_{2+}$ and $\beta_{2-}$ subunits (Fig. 1). In this case, movement of loop C was not as extensive as described for interfaces forming binding sites (both ortho- and allosteric), but a twist of its top part was observed. From the very beginning of the simulation a strong and stable interaction between the carboxyl group of Arg114$\gamma_2$ on loop A and the functional group of Arg129$\beta_2$ on loop E was present. This interaction is thus stabilizing the intersubunit coupling. Three other strong interactions appeared during the relaxation of the interface. Lys180$\beta_2$ from loop F moved toward the $\gamma_2$ subunit and formed an interaction with Glu150 from the β6 strand of this subunit, tightening the bottom area of the interface. Initially, the loop C top part showed some movements and loop A Arg114$\gamma_2$ dragged Ser217$\gamma_2$ and Thr216$\gamma_2$ downward closing the top part of the interface. Thus, the $\gamma_{2+}/\beta_{2-}$ interface becomes inaccessible for ligands as intra- and intersubunit interactions result in closure of the cavity. Notably, the molecular scenarios implemented in rendering the $\alpha_{1+}/\beta_{2-}$ and $\gamma_{2+}/\beta_{2-}$ interfaces inaccessible for ligands are strikingly different.

## Ion pore

As already mentioned, after release of constrains and removal of strychnine molecules the channel pore remained in a closed conformation and, as expected, movements associated with the relaxation within the TMD (Fig. 2B) were markedly smaller than in the ECD (Fig. 2A). In Fig. 7A, surface representation of water molecules in the ion pore is shown and the interruption of water filling the pore corresponds to the leucine hydrophobic gate. However, as we already pointed out, besides the selectivity filter yet another constriction point (but with higher radius) was found in the top area of the pore. This narrowing does not result from a deformation of the α helix but rather from positioning of the side chains of Glu270$\beta_2$, Lys274$\alpha_1$ and mostly of Glu285$\gamma_2$ (Fig. 7B) and can be easily crossed by water molecules, and thus is not visible in Fig. 7A. Since these residues, in contrast to hydrophobic leucine rings, are charged, it seemed interesting to check their interactions with the chloride ion. To this end, a chloride ion was docked at the centre of this site (with respect to the carbon α of five flanking residues) while the coordinates of the receptor and the rest of the system were taken from previous MD simulations in which a complete relaxation was achieved. The chloride ion was kept at the centre of the narrowing for 5 ns of simulation to allow for local equilibration of the system.

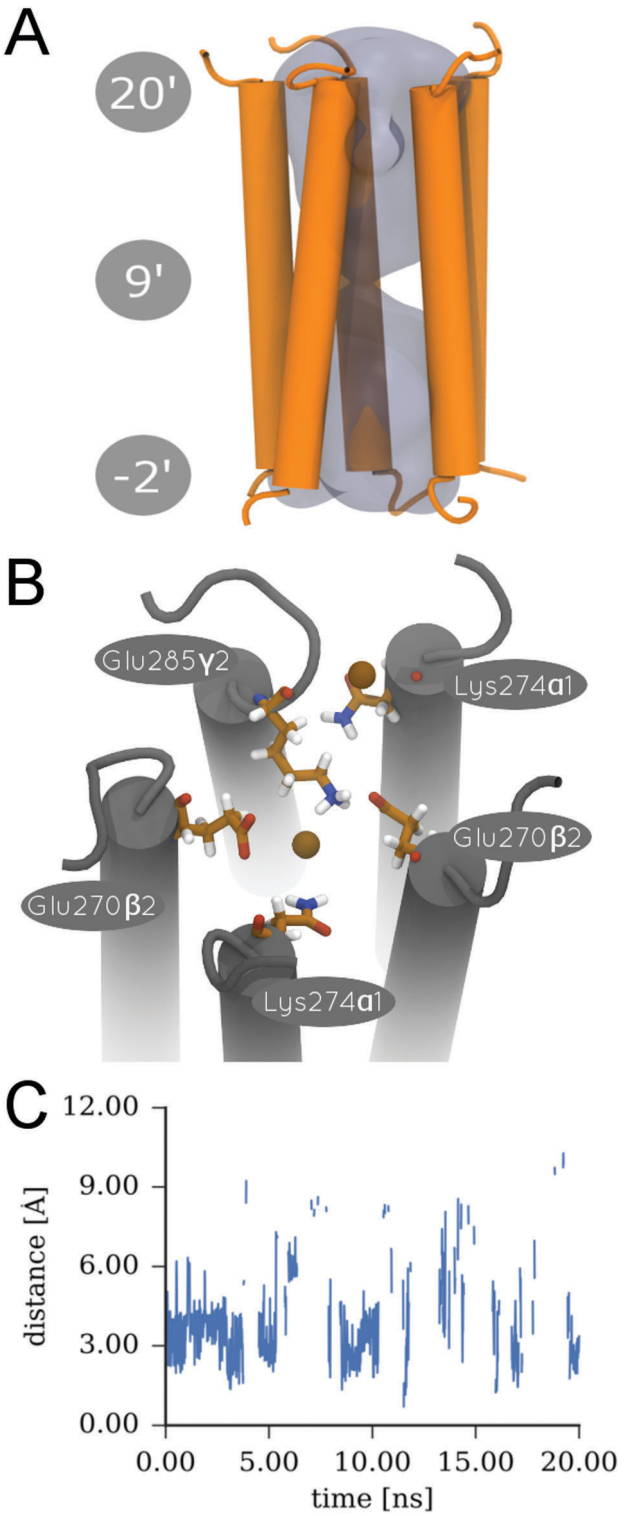


Fig. 7 Water and ion interactions in the TMD. (A) Five transmembrane helices (M2s) of respective subunits forming the ion pore depicted in orange. In the closed state the top and bottom areas of the pore are filled with water (represented with blue surface representation) but ion flow is blocked by the constriction point formed by leucine residues. (B) Top images are of the ion pore with chloride ion interaction with Glu270$\beta_2$, Lys274$\alpha_1$ and Glu285$\gamma_2$. The functional group of Glu285$\gamma_2$ points toward the centre of the pore. Another chloride ion is shown from the extracellular side of the receptor. (C) Distance between the chloride ion and centre of the residues forming the site. Only ions within 4 Å of any site residue were taken into account.

After releasing these constraints the chloride ion remained within 3.5 Å from this site for approximately another 5 ns and then moved up toward the ECD. Interestingly, after the loss of the ion, which was originally placed for 5 ns, another ion was trapped by this site. This situation is depicted in Fig. 7C where the ion averaged distance from the geometrical centre of the five α carbons is plotted against time (starting from the moment of releasing the equilibration constraints). The chloride ion remains relatively stable at this site for a few ns and then rapidly leaves it. When the distance between the ion and the site centre is less than 6 Å, the ion is considered to be still interacting with the site. Discontinuities in the line in Fig. 7C correspond to the fact that after one ion leaves the site, within 1 ns or so, another ion gets trapped by this site. Furthermore, after approximately 7.5 ns of unconstrained simulation, at the level of the chloride binding site a slight but evident expansion of α helices took place. This finding is depicted in Fig. 8A in which the area of the pentagon defined by the α-carbons is plotted against time. As seen in Fig. 8A, this α helix expansion occurred rapidly suggesting a conformation transition-like behaviour of the system. This structural change showed a high degree of stability (Fig. 8A) even if the ions showed some oscillatory movements in and out of the site (Fig. 7C). It needs to be emphasized that simulations of ion-pore interactions were carried out on the macromolecule structure which was fully relaxed in which no changes such as pore expansion took place without probing with the ion. Thus, these simulations indicate that pore expansion is a consequence of ion-pore interaction. Importantly, this change occurring at the level of the chloride ion site did not influence the main leucine constriction gate and the ion pore remained closed (Fig. 8B).

The pore profile in its stable conformation after the relaxation was compared to the profiles of other cys-loop family members (Fig. 8B). Interestingly, the here-described pore profile is similar to those of two other known structures: GluCl in 'apo' conformation and GlyR with strychnine in all binding sites (which was used as a template for the model). The minimum radius (at the 9′ leucine ring) of the here-considered model is 1.61 Å whereas the two mentioned receptors have constriction points equal to 1.28 Å and 1.35 Å, respectively. Despite the higher value of the gate radius in our model, chloride ions were not able to permeate through the pore. In particular, constriction at the top part of the ion pore is similar in our model and in the GlyR and GluCl 'apo' structures. Altogether, these data indicate a key role of chloride ions in shaping the TMD conformation.

## Discussion

In the present study we have considered a homology model for $\alpha_1\beta_2\gamma_2$ $GABA_AR$ (Fig. 2A, B and ESI,† Fig. S3B) in the closed conformation based on a template of the GlyR receptor with strychnine molecules bound to all five binding sites (Du *et al.* 2015, ESI,† Fig. S3A). Following relaxation after strychnine removal, the model was characterized by high stability and, most importantly, it nicely reproduced fundamental features of

 

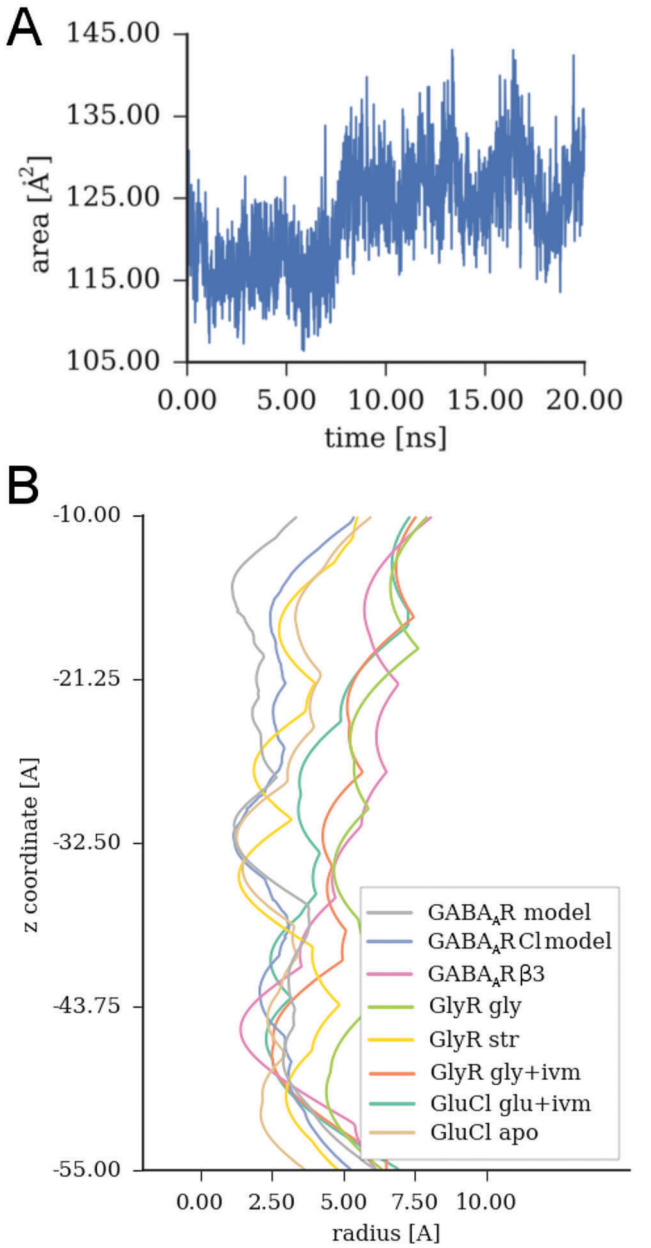


Fig. 8 Dimensions of the TMD's ion pore. (A) Area between α-carbons of residues forming the site of interaction with chloride ions shown in 6B. After approximately 7 ns of unconstrained simulation of ion-pore interaction a part of M2 α-helix formation underwent an expansion. (B) Comparison of published ion pore profiles within crystal structures of the cys-loop receptor family and the profile of the $GABA_AR$ homology model investigated in the present study. Narrowing in the middle of the pore is visible only in closed state structures. GlyR with glycine (gly), strychnine (str), glycine and ivermectin (gly + ivm),[10] GluCl with glutamate and ivermectin (glu + ivm)[12] and apo,[11] $GABA_AR$ $\beta_3$.[15]

this type $GABA_AR$ regarding the binding sites. It needs to be borne in mind that in spite of the heteropentameric structure, all five interfaces show a high degree of similarity making all of them potential binding sites. As described in the Results section only two orthosteric binding sites showed an open conformation, the allosteric one was partially open and the remaining interfaces were closed to the ligands and these model predictions reproduced the well-known features of this receptor type. Importantly, these properties were manifested in our molecular dynamics simulations spontaneously after strychnine removal without imposing any constraints on the putative binding sites or on any other part of the modelled macromolecule. Noteworthily, the relaxation process following strychnine removal encompassed large portions of the macromolecule in the vicinity of the binding sites as this antagonist molecule is large. Moreover, switching the homomeric template structure to a heteromeric one consisting of different $GABA_AR$ subunits was expected to give rise to substantial movements at the interfaces that indeed took place. In spite of this large potential for structural rearrangements upon relaxation, the model maintained its stability reaching a well-defined new equilibrium. These observations underscore the validity of our model which could be achieved most likely due to a relatively high homology between the $\alpha_1\beta_2\gamma_2$ $GABA_A$ receptor and the GlyR and the high quality of the GlyR structure determination.[10]

### Structural changes after strychnine removal

Many protein structures are co-crystallized with ligands *e.g.* $GABA_AR$ and benzamidine[15] or GlyR with glycine,[10] however in the latter case the ligand was not visible. Unbound structures are rarely resolved, *e.g.* nAChR,[16] thus information about the non-conducting state is mainly obtained from receptors with bound antagonists or channel blockers, rather than from ligand free receptors. In our study we present the closed and ligand-free $GABA_AR$ model which was obtained by removal of strychnine molecules from binding sites in the template GlyR structure. The strychnine molecule is markedly larger (molar mass 334.42 g × $mol^{-1}$) than GABA (103.120 g × $mol^{-1}$) or the physiological agonist of this receptor – glycine (75.07 g × $mol^{-1}$). The effect of ligand presence at the binding site has a strong impact on the local structure because of steric and electrostatic interactions between this molecule and residues in the vicinity of this site. Although our molecular dynamics simulations appear to faithfully reproduce the receptor structure in the closed and unbound conformation, it will be interesting to confront it with structures of highly homologous receptors (*e.g.* GlyR) resolved in the closed and ligand-free conformation.

One of our most important observations is that, at the orthosteric binding sites, loop C undergoes a movement defined here as vertical shift giving rise to binding site opening. This movement was observed from the very beginning of the simulation, including the protein energy minimization step, indicating the importance of this movement. Interestingly, in the ligand-free structure of the GLIC receptor, loop C was found to undergo vertical upward movement associated with widening of its upper part bearing striking similarity to what was observed at the orthosteric binding sites of our model. It needs to be pointed out, however, that in our model broadening of the upper part of loop C (in addition to the vertical shift) took place only at the binding site preceded by the $\alpha_1$ subunit due to interactions described in the Results section (Fig. 5A and B). A possible explanation for these structural rearrangements of

loop C in our model is that after ligand removal, specific interactions between the ligand molecule and binding site structure are replaced with less strictly defined interactions with solute molecules, allowing thus loop C to assume a more mobile structure. In general, opening of loop C, observed in orthosteric binding sites of our model, may be crucial for ligand binding allowing somehow easier ligand fit during the binding process or forming an energetically favourable path for the ligand from bulk solution to the binding site.[39] Loop C is well known to play an important role in binding site formation, interaction with the ligand molecule,[62,63] and other parts of the β subunit[64] and to be coupled with distant residues.[65] The results presented here underscore a crucial role of loop C in the process of ligand binding and may shed light on the molecular mechanisms of local and long-range interactions underlying conformational transitions of this receptor. Also, loop C is likely to play a significant role in signal transduction from the binding site to the channel gate,[60,61] but this process is beyond the timescale of the performed MD simulations. For this purpose creation of the $GABA_AR$ model in the bound open state is needed.

The behaviour of the modulatory binding site at the $\alpha_{1+}/\gamma_{2-}$ interface was different to that for the discussed orthosteric binding site. Oscillatory movements of loop C in this region may be related to the fact that ligand binding at this site is not necessary for receptor activation thus the binding path may have a different mechanism,[66] providing evidence that binding of modulators to the BDZ-site might affect the orthosteric binding sites. It cannot be thus excluded that modulation of $GABA_AR$ by agonists binding to the $\alpha_{1+}/\gamma_{2-}$ interface might affect also the above-mentioned orthosteric binding site asymmetry (see also below discussion on lateral intersubunit interactions).

### Asymmetry of intersubunit interfaces

The impact of strychnine molecule removal is not limited to orthosteric and allosteric binding sites as in the template structure all intersubunit interfaces were occupied by the antagonist, thus some relaxation processes were observed also at $\alpha_{1+}/\beta_{2-}$ and $\gamma_{2+}/\beta_{2-}$ interfaces (Fig. 5D). The most prominent difference between these two groups of interfaces is that in the first one the binding sites are opening or partially opening, while in the latter ones, a closure was observed (Fig. 5D). Two main structures involved in the respective movements are loop C (principal side of interface) and loop F (from the complementary side, Fig. 2A). In the case of GLIC receptors,[67] it has been consistently observed that in the non-active (vacant) conformation all binding sites at the interfaces are open (with characteristic C loop vertical shift) whereas in the active state, the interfaces show closed conformation. It seems thus worth emphasizing that the here-considered $GABA_AR$ shows a qualitative difference with respect to GLIC in the sense that only two out of 5 binding sites are fully open under the agonist-free conditions whereas the remaining ones are either partially open (modulatory site) or closed. This points to the importance of interactions between subunits within the heteromeric macromolecule in which structural asymmetry is accompanied by profound functional differences between the interfaces. It is also noteworthy that loop F exhibits a wide range of mobility and plays a role in binding affinity modulation,[68] thus it is not surprising that it is also an important player in the nonbinding interface.

In the $\alpha_{1+}/\beta_{2-}$ (Fig. 1) interface three residues were found to significantly contribute to interface forming: $Arg117\beta_2$, which is known to play a role in shaping the $\gamma_+/\beta_-$ interface (Goldschen-Ohm *et al.* 2004) and $Arg163\alpha_1$ that was positioning $Glu208\alpha_1$ to interact with $Arg117\beta_2$ (Fig. 6A). $Glu208\alpha_1$ in sequence alignment corresponds to $Ser204\beta_2$ that is known to be involved in binding/unbinding in the orthosteric binding site.[70,71] However, it seems that the nearby positioned $Arg207\beta_2$ is more important in creating the local network of interactions in which $Glu208\alpha_1$ (in our $GABA_AR$ model) was playing a key role. This arginine is also involved in the binding process[70–72] and, unlike $Ser204\beta_2$ is a charged residue although with reverse sign with respect to $Glu208\alpha_1$. Thus, in the orthosteric ligand binding interface, $Arg207\beta_2$ is involved in the binding of agonist molecules,[72] whereas in our model, $Glu208\alpha_1$, at the nonbinding interface, interacts with the complementary subunit, closing the site. This mechanism is accompanied by a network of interactions in the complementary subunit ($\beta_{2-}$). Key residues for this interaction are: $Arg169\beta_2$ interacting with $Asp171\beta_2$ which positions $Asp172\beta_2$ to form a salt bridge with $Lys192\beta_2$ (Fig. 6B). $Asp171\beta_2$ is a target of '$\beta_2$GKER' mutation[73,74] that is known to influence the assemblage of the receptor emphasizing the role of this residue in the intersubunit interactions. This interaction drags $Lys192\beta_2$, which is located on the β9 strand, affecting the GABA binding site (2nd binding site, Fig. 1), leading thus to asymmetry of orthosteric binding sites. The β9 strand is "pulled" by the bottom part of loop F and in this interaction a key role is played by attraction between Lys180β2 (loop F, '$\beta_2$GKER' mutation[73,74] and $Asp43\beta_2$ (on the strand β1)). The latter residue is known to play an important role in the $\beta_+/\alpha_-$ interface.[75]

In the second nonbinding interface, that is $\gamma_{2+}/\beta_2$ (Fig. 1), less interactions were observed. $Lys180\beta_2$ and $Glu150\gamma_2$ (Fig. 6C) pinned loop F toward loop C. Notably, $Glu150\gamma_2$ is also involved in benzodiazepine binding.[76] It can be thus hypothesized that the presence of a modulator at the modulatory binding site may affect the 1st GABA binding site (Fig. 1) *via* signalling transmitted through the chain of structures consisting of $Glu150\gamma_2$–$Lys180\beta_2$, β9 strand and loop C. Among other residues, important in this interface closure is also $Arg114\gamma_2$ (Fig. 6C) which plays a role in benzodiazepine binding.[76] This residue points its backbone group toward $Arg129\beta_2$ (Fig. 6C) forming electrostatic interaction. $Arg129\beta_2$ stacks with $Tyr62\beta_2$ (Fig. 6C) that is involved in muscimol binding at the $\alpha_{1+}/\beta_{2-}$ interface[77] and is homologous to $Phe64\alpha_1$, known to play an important role is transducing signals from the ECD to TMD.[78] It seems that this pathway may play a key role in receptor activation and modulation.

Taking altogether we propose the following possible mechanism of this orthosteric binding site inequality. The 1st binding site is separated from the 2nd binding site by two subunits ($\alpha_1$ and $\beta_2$, in the counter clockwise direction) and by three subunits ($\beta_2$, $\gamma_2$ and $\alpha_1$) in the clockwise direction (Fig. 1).

 

Our study indicates the counter clockwise interaction pathway because, besides shorter distance, only one closed intersubunit interface ($\alpha_{1+}/\beta_{2-}$) is present in this path. The second path consists of two interfaces: open, partially open modulatory binding site $\alpha_{1+}/\gamma_{2-}$ and one closed: $\gamma_{2+}/\beta_{2-}$ which is not only longer but involves open interfaces which are expected to be in a less tight conformation in comparison to the closed ones and therefore less suitable to transmit the lateral signal. Interestingly, in line with this suggestion, Sauguet[67] proposed that GLIC receptors in their closed conformation (*i.e.* with binding sites open) would be characterized by a higher flexibility, *i.e.* in a more ''loose'' structure which would be less prone to transmit mechanical signals. Thus, an empty open interface would inhibit binding site coupling in this direction path. We may speculate that the closure of the $\alpha_{1+}/\gamma_{2-}$ interface after modulator binding would enhance the coupling. Notably, some functional data indicated the non-equivalence of the two orthosteric binding sites in the $GABA_A$ receptor, although it is not consistent whether they show positive or negative cooperativity.[69,79,80]

### Chloride interaction site at the TMD

It is of note that in spite of substantial rearrangements following removal of strychnine molecules from the binding sites and structural adaptations at the subunit interfaces which have lost their symmetry present in the homomeric template, the channel pore maintained its closed conformation (Fig. 8B). Moreover, two ''classic'' constriction sites, one formed by the leucine ring at 9′ (the main channel gate in the closed state in the present model, Fig. 7A and 8B) and the second one related to the selectivity filter at the position 2′ (Fig. 7B), close to the cytoplasmic side of the pore were present in the considered model. A novel finding of the present study is that our MD simulations indicated the presence of a third ion constriction site in the top part of the TMD (Fig. 7B and 8B). Similar constriction rings were found in GlyR[10] where the narrowing is made of Ser20′ ring or in 5HT3R[13] where a hydrophilic ring in this region was reported. A similar constriction area was reported in other computational studies on $GABA_AR$,[81,82] but its functional impact was not examined. In our model this site is formed by a pentagon made of Glu270$\beta_2$, Lys274$\alpha_1$ and Glu285$\gamma_2$ (20′ residue level, Fig. 2B and 7B). Thus, in contrast to the 9′ leucine gate, this site is made of charged residues and respective subunits contribute with different residue types reflecting thus the structure asymmetry as it was already pointed out for ECD interfaces. The importance of this region for ion conduction is emphasized by Di Maio *et al.*[83] who found in their computational studies that electrostatic interactions in the homologous area of the 5HT3 receptor gave rise to substantial differences for energy of ion passage through the pore in the case of sodium and chloride ions. Our results show that this region in the $GABA_AR$ plays a particular role in interacting with chloride ions. Moreover, we found that this interaction occurs in two directions as the pore undergoes an expansion as a result of interaction with chloride ions. Thus, our data confirm the notion that the channel macromolecule including its pore is not a rigid structure that purely passively permeates ions but rather it interacts with solute components changing its local structure and function. Our simulations predict that when chloride ion-pore interaction is sufficiently intense (Fig. 7C), the pore expansion occurs (Fig. 8A) in the closed state without affecting the main (leucine) channel gate (Fig. 8B). We may thus speculate that the role of this 20′ site is to 'preactivate' the pore before opening. It is expected that in the case of the open channel pore when chloride ions are abundantly present in the pore, this expansion will be also present although verification of this hypothesis would require simulations in the open conformation. Experimental findings that glycine and $GABA_A$ receptor kinetics strongly depend on anion concentration[84–86] are consistent with the notion that ion-pore interaction may affect the channel functioning. Another possible role of pore expansion could be to affect the channel conductance. Interestingly, whereas the main channel gate is made of conserved residues (among different subunits), 20′ constriction composition depends on assembly type, which is known to influence channel conductance.[87] Our simulations showed prominent influence of Glu285$\gamma_2$ on this site and it would be interesting to check the impact of this residue on the channel conductance as, in general, the presence of the $\gamma_2$ subunit strongly influences this parameter (higher conductance of $\alpha_1\beta_1\gamma_2$ $GABA_AR$ compared to $\alpha_1\beta_1$ $GABA_AR$[88]). Thus, we propose that this site might stabilize the pore and shape the channel conductance.

We conclude that the here-proposed homology model of heteropentameric $GABA_AR$ confirms major features of this receptor and sheds new light on the molecular features of binding sites, non-binding interfaces and the pore region. In particular, we report that lateral interactions between subunit structures appear particularly important in setting the communication mechanisms between orthosteric and modulatory sites. This study highlights also the fact that heteropentameric structures offer a greater functional versatility due to local interactions enabling different interfaces to assume different functions.

## Acknowledgements

This work was supported by National Science Centre, Poland, under grant ''MAESTRO'' UMO-2015/18/A/NZ1/00395. This research was supported in part by PLGrid Infrastructure. Calculations have been carried out in part using resources provided by Wroclaw Centre for Networking and Supercomputing (http://wcss.pl/), grant no. 274. S. K. gratefully acknowledges statutory funds from Department of Biomedical Engineering at Wroclaw University of Science and Technology.

## Notes and references

1 H. Betz, Ligand-gated ion channels in the brain: The amino acid receptor superfamily, *Neuron*, 1990, **5**, 383–392.
2 E. Sigel and M. E. Steinmann, Structure, function, and modulation of GABA(A) receptors, *J. Biol. Chem.*, 2012, **287**, 40224–40231.

3 R. M. McKernan and P. J. Whiting, Which GABAA-receptor subtypes really occur in the brain?, *Trends Neurosci.*, 1996, **19**, 139–143.

4 S. J. Farrar, P. J. Whiting, T. P. Bonnert and R. M. McKernan, Stoichiometry of a Ligand-gated Ion Channel Determined by Fluorescence Energy Transfer, *J. Biol. Chem.*, 1999, **274**, 10100–10104.

5 W. Olsen and J. Tobin, Molecular biology of GABAA receptors, *FASEB J.*, 1990, **4**, 1469–1480.

6 R. L. Macdonald, R. W. Olsen and G. R. Channels, GABAA receptor channels, *Annu. Rev. Neurosci.*, 1994, **17**, 569–602.

7 J. W. Mozrzymas, Dynamism of GABAA receptor activation shapes the 'personality' of inhibitory synapses, *Neuropharmacology*, 2004, **47**, 945–960.

8 A. Barberis, E. M. Petrini and J. W. Mozrzymas, Impact of synaptic neurotransmitter concentration time course on the kinetics and pharmacological modulation of inhibitory synaptic currents, *Front. Cell. Neurosci.*, 2011, **5**, 6.

9 X. Huang, H. Chen, K. Michelsen, S. Schneider and P. L. Shaffer, Crystal structure of human glycine receptor-α3 bound to antagonist strychnine, *Nature*, 2015, **526**, 277–280.

10 J. Du, W. Lü, S. Wu, Y. Cheng and E. Gouaux, Glycine receptor mechanism elucidated by electron cryo-microscopy, *Nature*, 2015, **526**, 224–229.

11 T. R. Althoff, E. Hibbs, S. Banerjee and E. Gouaux, X-ray structures of GluCl in apo states reveal a gating mechanism of Cys-loop receptors, *Nature*, 2014, **512**, 333–337.

12 R. Hibbs and E. Gouaux, Principles of activation and permeation in an anion-selective Cys-loop receptor, *Nature*, 2011, **474**, 54–60.

13 G. Hassaine, C. Deluz, L. Grasso, R. Wyss, M. B. Tol, R. Hovius, A. Graff, H. Stahlberg, T. Tomizaki, A. Desmyter, C. Moreau, X. Li, F. Poitevin, H. Vogel and H. Nury, X-ray structure of the mouse serotonin 5-HT3 receptor, *Nature*, 2014, **512**, 276–281.

14 M. Kudryashev, *et al.*, The Structure of the Mouse Serotonin 5-HT3 Receptor in Lipid Vesicles, *Structure*, 2016, **24**, 165–170.

15 P. S. Miller and A. R. Aricescu, Crystal structure of a human GABAA receptor, *Nature*, 2014, **512**, 270–275.

16 N. Unwin, Refined structure of the nicotinic acetylcholine receptor at 4 A resolution, *J. Mol. Biol.*, 2005, **346**, 967–989.

17 R. L. Macdonald, C. J. Rogers, R. E. Twyman, C. J. Rogers and R. L. Macdonald, Kinetic Properties Of The Gabaa Receptor Main Conductance State Of Mouse Spinal Cord Neurones In Culture By, *J. Physiol.*, 1989, **28**, 193–220.

18 D. S. Weiss and K. L. Magleby, Gating scheme for single GABA-activated Cl- channels determined from stability plots, dwell-time distributions and adjacent-interval durations, *J. Neurosci.*, 1989, **9**, 1314–1324.

19 D. J. Maconochie, J. M. Zempel and J. H. Steinbach, How quickly can GABAA receptors open?, *Neuron*, 1994, **12**, 61–71.

20 M. V. Jones, Y. Sahara, J. A. Dzubay and G. L. Westbrook, Defining affinity with the GABAA receptor, *J. Neurosci.*, 1998, **18**, 8590–8604.

21 T. A. Verdoorn, A. Draguhn, S. Ymer, P. H. Seeburg and B. Sakmann, Functional properties of recombinant rat GABAA receptors depend upon subunit composition, *Neuron*, 1990, **4**, 919–928.

22 W. Sieghart and G. Sperk, Subunit Composition, Distribution and Function of GABA, *Curr. Top. Med. Chem.*, 2002, **2**, 795–816.

23 U. Rudolph and H. Mohler, GABAA Receptor Subtypes: Therapeutic Potential in Down Syndrome, Affective Disorders, Schizophrenia and Autism, *Annu. Rev. Pharmacol. Toxicol.*, 2014, **54**, 483–507.

24 E. Sigel, *et al.*, Point mutations affecting antagonist affinity and agonist dependent gating of GABAA receptor channels, *EMBO J.*, 1992, **11**, 2017–2023.

25 A. Buhr, M. T. Schaerer, R. Baur and E. Sigel, Residues at positions 206 and 209 of the alpha1 subunit of gamma-aminobutyric AcidA receptors influence affinities for benzodiazepine binding site ligands, *Mol. Pharmacol.*, 1997, **52**, 676–682.

26 B. Vafa and P. R. Schofield, Heritable Mutations in the Glycine, GABAA/and Nicotinic Acetylcholine Receptors Provide New Insights into The Ligand-Gated Ion Channel Receptor Superfamily, *Int. Rev. Neurobiol.*, 1998, **42**, 285–332.

27 B. X. Carlson, A. C. Engblom, U. Kristiansen, A. Schousboe and R. W. Olsen, A single glycine residue at the entrance to the first membrane-spanning domain of the gamma-aminobutyric acid type A receptor beta(2) subunit affects allosteric sensitivity to GABA and anesthetics, *Mol. Pharmacol.*, 2000, **57**, 474–484.

28 M. D. Krasowski, K. Nishikawa, N. Nikolaeva, A. Lin and N. L. Harrison, Methionine 286 in transmembrane domain 3 of the GABAA receptor B subunit controls a binding cavity for propofol and other alkylphenol general anesthetics, *Neuropharmacology*, 2001, **41**, 952–964.

29 K. Brejc, *et al.*, Crystal structure of an ACh-binding protein reveals the ligand-binding domain of nicotinic receptors, *Nature*, 2001, **411**, 269–276.

30 A. Miyazawa, Y. Fujiyoshi and N. Unwin, Structure and gating mechanism of the acetylcholine receptor pore, *Nature*, 2003, **423**, 949–955.

31 R. J. C. Hilf and R. Dutzler, X-ray structure of a prokaryotic pentameric ligand-gated ion channel, *Nature*, 2008, **452**, 375–379.

32 N. Bocquet, *et al.*, X-ray structure of a pentameric ligand-gated ion channel in an apparently open conformation, *Nature*, 2009, **457**, 111–114.

33 S. S. Jayakar, *et al.*, Multiple propofol-binding sites in a γ-aminobutyric acid type a receptor ($GABA_AR$) identified using a photoreactive propofol analog, *J. Biol. Chem.*, 2014, **289**, 27456–27468.

34 S. S. Jayakar, *et al.*, Positive and Negative Allosteric Modulation of an alpha1beta3gamma2 gamma-Aminobutyric Acid Type A (GABAA) Receptor by Binding to a Site in the Transmembrane Domain at the $gamma^+$/-$beta^-$ Interface, *J. Biol. Chem.*, 2015, **290**, 23432–23446.


 

35 R. Bergmann, K. Kongsbak, P. L. Sørensen, T. Sander and T. Balle, A Unified Model of the GABAA Receptor Comprising Agonist and Benzodiazepine Binding Sites, *PLoS One*, 2013, **8**, e52323.

36 M. Wallner, H. J. Hanchar and R. W. Olsen, Alcohol selectivity of B3-containing GABAA receptors: Evidence for a unique extracellular alcohol/imidazobenzodiazepine Ro15-4513 binding site at the a + B-subunit interface in aB3d GABAa receptors, *Neurochem. Res.*, 2014, **39**, 1118–1126.

37 J. A. Ashby, *et al.*, GABA binding to an insect GABA receptor: a molecular dynamics and mutagenesis study, *Biophys. J.*, 2012, **103**, 2071–2081.

38 T. Sander, *et al.*, New insights into the GABA A receptor structure and orthosteric ligand binding: Receptor modeling guided by experimental data, *Proteins: Struct., Funct., Bioinf.*, 2011, **79**, 1458–1477.

39 T. S. Carpenter and F. C. Lightstone, An Electrostatic Funnel in the GABA-Binding Pathway, *PLoS Comput. Biol.*, 2016, **12**, e1004831.

40 A. Bateman, *et al.*, UniProt: A hub for protein information, *Nucleic Acids Res.*, 2015, **43**, D204–D212.

41 H. M. Berman, *et al.*, The Protein Data Bank, *Nucleic Acids Res.*, 2000, **28**, 235–242.

42 F. Sievers, *et al.*, Fast, scalable generation of high-quality protein multiple sequence alignments using Clustal Omega, *Mol. Syst. Biol.*, 2011, **7**, 539.

43 A. Drozdetskiy, C. Cole, J. Procter and G. J. Barton, JPred4: A protein secondary structure prediction server, *Nucleic Acids Res.*, 2015, **43**, W389–W394.

44 B. Webb and A. Sali, Comparative protein structure modeling using MODELLER, *Current Protocols in Bioinformatics*, 2014, vol. 2014.

45 P. Benkert, M. Künzli and T. Schwede, QMEAN server for protein model quality estimation, *Nucleic Acids Res.*, 2009, **37**, 510–514.

46 S. C. Lovell, *et al.*, Structure validation by C alpha geometry: phi,psi and C beta deviation, *Proteins: Struct., Funct., Bioinf.*, 2003, **50**, 437–450.

47 S. Jo, T. Kim, V. G. Iyer and W. Im, CHARMM-GUI: A Web-Based Graphical User Interface for CHARMM, *J. Comput. Chem.*, 2008, **29**, 1859–1865.

48 J. Lee, *et al.*, CHARMM-GUI Input Generator for NAMD, GROMACS, AMBER, OpenMM, and CHARMM/OpenMM Simulations Using the CHARMM36 Additive Force Field, *J. Chem. Theory Comput.*, 2016, **12**, 405–413.

49 J. C. Phillips, *et al.*, Scalable molecular dynamics with NAMD, *J. Comput. Chem.*, 2005, **26**, 1781–1802.

50 W. L. Jorgensen, J. Chandrasekhar, J. D. Madura, R. W. Impey and M. L. Klein, Comparison of simple potential functions for simulating liquid water, *J. Chem. Phys.*, 1983, **79**, 926.

51 S. R. Durell, B. R. Brooks and A. Ben-Naim, Solvent-Induced Forces between Two Hydrophilic Groups, *J. Phys. Chem.*, 1994, **98**, 2198–2202.

52 O. Trott and A. J. Olson, AutoDock Vina: Improving the Speed and Accuracy of Docking with a New Scoring Function, Efficient Optimization, and Multithreading, *J. Comput. Chem.*, 2010, **31**, 2967–2970.

53 W. Humphrey, A. Dalke and K. Schulten, VMD: visual molecular dynamics, *J. Mol. Graphics*, 1996, **14**, 33–38.

54 S. Van Der Walt, S. C. Colbert and G. Varoquaux, The NumPy array: A structure for efficient numerical computation, *Comput. Sci. Eng.*, 2011, **13**, 22–30.

55 W. McKinney, Data Structures for Statistical Computing in Python, *Proceedings of the 9th Python in Science Conference*, 2010, pp. 51–56.

56 J. D. Hunter, Matplotlib: A 2D graphics environment, *Comput. Sci. Eng.*, 2007, **9**, 99–104.

57 M. Waskom, *et al.* seaborn: v0.7.0 (January 2016) 2016, DOI:10.5281/zenodo.45133.

58 O. S. Smart, J. G. Neduvelil, X. Wang, B. A. Wallace and M. S. P. Sansom, HOLE: A program for the analysis of the pore dimensions of ion channel structural models, *J. Mol. Graphics*, 1996, **14**, 354–360.

59 M. Nys, D. Kesters and C. Ulens, Structural insights into Cys-loop receptor function and ligand recognition, *Biochem. Pharmacol.*, 2013, **86**, 1042–1053.

60 P. Purohit and A. Auerbach, Loop C and the mechanism of acetylcholine receptor-channel gating, *J. Gen. Physiol.*, 2013, **141**, 467–478.

61 R. Vij, P. Purohit and A. Auerbach, Modal affinities of endplate acetylcholine receptors caused by loop C mutations, *J. Gen. Physiol.*, 2015, **146**, 375–386.

62 P. Purohit, I. Bruhova, S. Gupta and A. Auerbach, Catch-and-hold activation of muscle acetylcholine receptors having transmitter binding site mutations, *Biophys. J.*, 2014, **107**, 88–99.

63 S. P. Venkatachalan and C. Czajkowski, A conserved salt bridge critical for GABA(A) receptor function and loop C dynamics, *Proc. Natl. Acad. Sci. U. S. A.*, 2008, **105**, 13604–13609.

64 P. N. Tran, K. T. Laha and D. A. Wagner, A tight coupling between $\beta_2$Y97 and $\beta_2$F200 of the GABA(A) receptor mediates GABA binding, *J. Neurochem.*, 2011, **119**, 283–293.

65 K. R. Gleitsman, J. A. P. Shanata, S. J. Frazier, H. A. Lester and D. A. Dougherty, Long-range coupling in an allosteric receptor revealed by mutant cycle analysis, *Biophys. J.*, 2009, **96**, 3168–3178.

66 F. Sancar and C. Czajkowski, Allosteric modulators induce distinct movements at the GABA-binding site interface of the GABA-A receptor, *Neuropharmacology*, 2011, **60**, 520–528.

67 L. Sauguet, *et al.*, Crystal structures of a pentameric ligand-gated ion channel provide a mechanism for activation, *Proc. Natl. Acad. Sci. U. S. A.*, 2014, **111**, 966–971.

68 T. S. Carpenter, E. Y. Lau and F. C. Lightstone, A role for loop F in modulating GABA binding affinity in the GABA(A) receptor, *J. Mol. Biol.*, 2012, **422**, 310–323.

69 M. P. Goldschen-ohm, D. A. Wagner, S. Petrou and M. V. Jones, An Epilepsy-Related Region in the GABAA Receptor Mediates Long-Distance Effects on GABA and Benzodiazepine Binding Sites, *Mol. Pharmacol.*, 2010, **77**, 35–45.

70 D. A. Wagner, C. Czajkowski and M. V. Jones, An arginine involved in GABA binding and unbinding but not gating of the GABA(A) receptor, *J. Neurosci.*, 2004, **24**, 2733–2741.

71 C. Czajkowski and D. A. Wagner, Structure and dynamics of the GABA binding pocket: A narrowing cleft that constricts during activation, *J. Neurosci.*, 2001, **21**, 67–74.
72 M. P. Goldschen-Ohm, D. A. Wagner and M. V. Jones, Three arginines in the GABAA receptor binding pocket have distinct roles in the formation and stability of agonist- *versus* antagonist-bound complexes, *Mol. Pharmacol.*, 2011, **80**, 647–656.
73 P. M. Taylor, *et al.*, Identification of amino acid residues within GABA(A) receptor beta subunits that mediate both homomeric and heteromeric receptor expression, *J. Neurosci.*, 1999, **19**, 6360–6371.
74 K. Bollan, *et al.*, GABAA receptor composition is determined by distinct assembly signals within a and b subunits, *J. Biol. Chem.*, 2003, **278**, 4747–4755.
75 D. T. Baptista-Hon, A. Krah, U. Zachariae and T. G. Hales, A role for loop G in the α1 strand in GABAA receptor activation, *J. Physiol.*, 2016, **594**, 5555–5571.
76 A. J. Boileau, A. M. Kucken, A. R. Eevers and C. Czajkowski, Molecular Dissection of Benzodiazepine Binding and Allosteric Coupling Using Chimeric γ-Aminobutyric Acid A Receptor Subunits, *Mol. Pharmacol.*, 1998, **303**, 295–303.
77 R. Baur and E. Sigel, On high- and low-affinity agonist sites in GABAA receptors, *J. Neurochem.*, 2003, **87**, 325–332.
78 M. Szczot, M. Kisiel, M. M. Czyzewska and J. W. Mozrzymas, α1F64 Residue at GABA(A) receptor binding site is involved in gating by influencing the receptor flipping transitions, *J. Neurosci.*, 2014, **34**, 3193–3209.
79 D. Maric, *et al.*, GABAA receptor subunit composition and functional properties of Cl-channels with differential sensitivity to zolpidem in embryonic rat hippocampal cells, *J. Neurosci.*, 1999, **19**, 4921–4937.
80 J. W. Mozrzymas, A. Barberis, K. Mercik and E. D. Zarnowska, Binding Sites, Singly Bound States, Conformation Coupling Shape GABA-Evoked Currents, *J. Neurophysiol.*, 2003, **89**, 871–883.
81 R. S. K. Vijayan, *et al.*, Modeling the Closed and Open State Conformations of the GABA, *J. Chem. Inf. Model.*, 2012, **52**, 2958–2969.
82 A. V. Rossokhin and B. S. Zhorov, Side chain flexibility and the pore dimensions in the GABAA receptor, *J. Comput.-Aided Mol. Des.*, 2016, **30**, 559–567.
83 D. Di Maio, B. Chandramouli and G. Brancato, Pathways and barriers for ion translocation through the 5-HT3A receptor channel, *PLoS One*, 2015, **10**, 1–23.
84 S. J. Pitt, L. G. Sivilotti and M. Beato, High Intracellular Chloride Slows the Decay of Glycinergic Currents, *J. Neurosci.*, 2009, **28**, 11454–11467.
85 M. Moroni, *et al.*, Chloride ions in the pore of glycine and GABA channels shape the time course and voltage dependence of agonist currents, *J. Neurosci.*, 2011, **31**, 14095–14106.
86 C. M. Houston, D. P. Bright, L. G. Sivilotti, M. Beato and T. G. Smart, Intracellular Chloride Ions Regulate the Time Course of GABA-Mediated Inhibitory Synaptic Transmission, *J. Neurosci.*, 2009, **29**, 10416–10423.
87 D. A. Mathers, Activation and inactivation of the GABA(A) receptor: Insights from comparison of native and recombinant subunit assemblies, *Can. J. Physiol. Pharmacol.*, 1991, **69**, 1057–1063.
88 T. P. Angelotti and R. L. Macdonald, Assembly of GABAA receptor subunits: alpha 1 beta 1 and alpha 1 beta 1 gamma 2S subunits produce unique ion channels with dissimilar single-channel properties, *J. Neurosci.*, 1993, **13**, 1429–1440.

 